Protein-Induced Surface Structuring in Myelin Membrane Monolayers

Carla M. Rosetti and Bruno Maggio
Centro de Investigaciones en Química Biológica de Córdoba, Departamento de Química Biológica, Facultad de Ciencias Químicas, Universidad Nacional de Córdoba, Ciudad Universitaria, Córdoba, Argentina

ABSTRACT Monolayers prepared from myelin conserve all the compositional complexity of the natural membrane when spread at the air-water interface. They show a complex pressure-dependent surface pattern that, on compression, changes from the coexistence of two liquid phases to a viscous fractal phase embedded in a liquid phase. We dissected the role of major myelin protein components, myelin basic protein (MBP), and Folch-Lees proteolipid protein (PLP) as crucial factors determining the structural dynamics of the interface. By analyzing mixtures of a single protein with the myelin lipids we found that MBP and PLP have different surface pressure-dependent behaviors. MBP stabilizes the segregation of two liquid phases at low pressures and becomes excluded from the film under compression, remaining adjacent to the interface. PLP, on the contrary, organizes a fractal-like pattern at all surface pressures when included in a monolayer of the protein-free myelin lipids but it remains mixed in the MBP-induced liquid phase. The resultant surface topography and dynamics is regulated by combined near to equilibrium and out-of-equilibrium effects. PLP appears to act as a surface skeleton for the whole components whereas MBP couples the structuring to surface pressure-dependent extrusion and adsorption processes.

INTRODUCTION

Biological membranes are complex fluids constituted by a wide variety of lipids and proteins whose thermodynamic and/or structural compatibilities inherently lead to many possible manners of organization. It is generally accepted that biological membranes are spatially inhomogeneous (1–3) and an important biological role has been attributed to this property as a mechanism for conveying information among different levels of organization (4–9). Some mechanisms involved in maintaining the heterogeneity such as phase transitions (10), nonideal mixing in binary mixtures (11,12), Ca^{2+} binding in charged membranes (13,14), among others, have been identified in simple systems. Membrane proteins, formerly mostly conceived as preferentially partitioning in preassembled lipid domains are increasingly recognized as fundamental structuring factors driving lateral heterogeneity. Proteins are known to mediate the formation of domains through electrostatic lipid-protein interactions (15,16), exclusion or partition into cholesterol enriched phases (17), and through hydrophobic mismatch (18). Likely, in natural membranes these phenomena are also determinants of the inhomogeneous distribution of components but the study of complex systems becomes difficult with the growing number of variables escaping precise control. Monomolecular layers prepared from whole natural membranes enable one to study some aspects of complex systems. However, since the asymmetric arrangement of the lipids and proteins is lost and the thickness is reduced to one hemilayer, no direct extrapolation of the results obtained in monolayers to the behavior of the natural bilayer membrane is possible. In spite of that, these systems, having the compositional complexity of the whole natural membranes, can be studied under controlled conditions of packing, surface pressure, surface potential (19,20), and at the same time, permit one to relatively manipulate the composition while directly observing the surface topography (21). The role of some protein and lipid components has been explored recently in native pulmonary surfactant monolayers (22,23).

Monomolecular layers from the isolated bovine spinal cord whole myelin have been previously described (20). Myelin membranes can be obtained with high purity and are quite unique in that the lipid/protein ratio is higher than in other cellular membranes. The lipid fraction is represented by ~40% cholesterol and it is much enriched in sphingolipids, namely sphingomyelin, galactocerebroside, and sulfatide. Two major basic proteins represent ~80% by weight of the whole protein fraction: the amphitropic myelin basic protein (MBP) and the hydrophobic transmembrane Folch-Lees proteolipid protein (PLP); both have important structural roles in myelin membrane organization (24,25). The whole myelin membrane is soluble in chloroform/methanol and can be spread at the air-water interface as a monolayer with the same composition of the original membrane and conserving the surface behavior and topography of films spread from aqueous dispersion of myelin vesicles (20,21). The surface pattern of myelin monolayers is characterized by two coexisting liquid phases at low surface pressure; at high surface pressures a continuous viscous phase, which is embedded in a liquid phase, self-organizes as a fractal structure. This is characterized by self similar patterns extending over a scale ranging from micrometers to millimeters, with a fractal dimension of 1.7 (21,26). Over the whole compression range the phase coexistence involves lateral segregation of some lipid components (such as cholesterol, galactocerebroside,

Submitted May 14, 2007, and accepted for publication July 13, 2007.

Address reprint requests to Bruno Maggio, E-mail: bmaggio@dqb.fcq.unc.edu.ar.

Editor: Michael Edidin.

0006-3495/07/12/4254/14 $2.00

doi: 10.1529/biophysj.107.112441

and phosphatidylserine) in liquid ordered domains separated from others containing the major myelin proteins (PLP and MBP) together with other lipids (i.e., such as ganglioside GM1) (27). Previous results on interfacial films prepared from myelin lipid fractions that contained PLP as the sole protein species, allowed one to conclude that the myelin lipids were responsible for liquid phase coexistence, stable only up to very low surface pressures, whereas the presence of PLP induced fractal structures with a fractal dimension of 1.6 (28). In this work we have dissected the thermodynamic and topographic variations induced by the purified major myelin proteins (PLP and MBP) on monolayers formed by the protein-free whole myelin lipid fraction. The results show that, individually or in combination, both proteins constitute major structuring factors accounting for the surface topography of whole myelin monolayers. The self-structuring of the interface is a result of an out-of-equilibrium organization driven by PLP and a near-equilibrium surface organization induced by MBP. We were also able to partially correlate the topographic and thermodynamic behavior of this complex mixture.

MATERIAL AND METHODS

Myelin fractions

The isolation of the protein-free myelin lipid fraction, containing almost all the myelin lipids (except gangliosides) was previously described (28). Briefly, purified bovine spinal cord whole myelin was solubilized in 19 vol of chloroform/methanol (2:1, v/v). Whole myelin is initially fully soluble in this medium (high molecular weight proteins, such as the Wolfgram proteins, subsequently aggregate slowly with time). A Folch's partition of the extract is immediately performed by the addition of 1/5 vol of water that results in two sharply separated lower and upper clear immiscible solvent phases (respectively, representing a proportion of 3:7 v/v). The upper phase (containing the gangliosides), together with the two-phase interface (in which the MBP and Wolfgram proteins are accumulated) were discarded. The lower phase (chloroform/methanol/water 86:14:1), which contains over 98% of all the major myelin lipids and PLP as the sole protein component, was washed twice with an upper solvent solution prepared by mixing the pure solvents in the same proportions as the experimental upper solvent phase (chloroform/methanol/water 3:48:47). Finally, PLP is rendered insoluble after equilibration of the lower solvent phase (in proportion 1:1) with upper solvent solution containing 0.1 M potassium citrate. PLP accumulates at the interface and was discarded. The procedure is repeated three times and ultimately the lower phase is washed with a citrate-free upper phase (in proportion 1:1). The amount of PLP remaining in the final extract was below 1.1×10^{-2} mol % with respect to total lipids. According to high performance liquid chromatography (HPTLC, running solvent, chloroform/methanol/water 70:30:4 revealed with 3% cupric acetate/8% ortophosphoric acid) the composition of the total lipid extract matches that of whole myelin.

MBP and PLP purification procedure

To obtain myelin basic protein we followed a purification procedure previously employed (29). Bovine spinal cord was grinded in a chloroform/methanol 2:1 solution (0.5 g/ml) and stirred overnight at 4°C. The solution was filtered and the retained material was further dispersed in chloroform/methanol 2:1 (0.1 g/ml). After repeating the procedure three times, the retained material was resuspended in acetone (0.1 g/ml), filtered, dispersed in milli-Q water (0.05 g/ml), and stirred overnight at 4°C. The aqueous dispersion, after filtering and resuspension in milli-Q water (0.2 g/ml), was titrated to pH 3 with hydrochloric acid under stirring. The pH 3 solution, where the MBP becomes soluble, was filtered and the pellet was discarded. The pH 3 extract was lyophilized and resuspended in hydrochloric acid 0.01 M/acetic acid 1 M/sucrose 20% 1:1:1. This resuspended material was passed through a Sephadex G100 column (2.8 × 92 cm column for 150 mg of protein) previously equilibrated with hydrochloric acid 0.01 M. Elution was carried out with hydrochloric acid 0.01 M and the fractions containing protein, as detected by absorbance at 225 nm were collected, pooled, and lyophilized.

We obtained Folch-Lees proteolipid as previously described (30). Bovine brain white matter was grinded in 19 vol of chloroform/methanol 2:1, filtered and 0.2 vol of KCl 0.1 M was added to the eluted solution. After mixing, the emulsion separates into two solvent phases under standing, with the lower phase containing the PLP. This phase was washed and equilibrated six times with upper solvent phase (chloroform/methanol/water 3:48:47). After reducing the volume to half of the original (under a nitrogen flux), it was cooled to 4°C and precipitated with 4 vol of ethyl ether. The insoluble material was washed twice with methanol/acetic acid (100:1), and solubilized in chloroform/methanol/acetic acid (50:50:1). The latter solution was passed trough a Sephadex LH20 column and the eluted fractions with the first protein peak were collected and passed again through Sephadex LH20. The Folch Lees proteolipid obtained contains <1.55 μg of Pi/mg of protein and 30 μg of sulfatide/mg of protein.

SDS-PAGE of the purified protein fractions showed bands running with a molecular weight (MW) of 18,500 for MBP and 25,000 for PLP, in agreement with literature (although the MW accepted for PLP is 29,000, it usually runs as a lighter MW band in these systems (24)).

Fluorescence and Brewster angle microscopy

Monolayer microscopy images were taken in real time while simultaneously recording isothermal compression of the film. The setup consisted of a Langmuir balance (KSV minithrough equipment, Helsinki, Finland, or KIBRON microtrough, Helsinki, Finland) mounted on the stage of a Zeiss Axiovert or Axioplan (Carl Zeiss, Oberkochem, Germany) fluorescence microscope, and/or a miniBAM (Nanofilm Technologies, Gottingem, Germany), as previously described (28).

For observations with the miniBAM, the surface was illuminated with a 658-nm p-polarized light from a 30-mW laser diode at the Brewster angle of the bare interface (from which a minimum of reflectance is achieved) and the reflected light was collected with a standard achromat (12.5-mm diameter, 25-mm focus). When a film is spread on the aqueous subphase it acts as a third optical medium and reflects light depending on its local thickness and refractive index.

The gray level signal of our camera is linearly related to the light intensity for 1/500 shutter speed at least up to 160 gray arbitrary units. The relative reflectance I can be derived ($r^2 = 0.99$) from:

$$I = -0.915 \times 10^{-6} + (4.502 \times 10^{-8})\, GL, \qquad (1)$$

where GL is the gray level in arbitrary units (31).

Gray level measurements were taken at the maximum illumination area of the bell-shaped light intensity distribution. The mean value of 10 × 10 pixels sections (83 × 83 μm) was measured. These values were reproducible from one experiment to another ($\pm$10 arbitrary units).

For fluorescence observation, lipid or lipid-protein solutions were doped with 0.8 mol % of *N*-(lissamine rhodamine B-sulfonyl) diacyl-*sn*-glycero-3-phosphatidylethanolamine (Rho-egg PE) with 55% of unsaturated acyl chains or 1 mol % *N*-(7-nitro-2-1,3-benzoxadiazol-4-yl) dipalmitoyl-*sn*-glycero-3-phosphoethanolamine (NBD-DPPE) (Avanti Polar Lipids, Alabaster, AL). After spreading onto a TRIS-Ca buffer PH 7.4 (10 mM Tris, 100 mM NaCl, 20 mM $CaCl_2$), the solvent was allowed to evaporate for 10 min. Films were imaged during isometric compression with a charge-coupled device video camera Zeiss or a Micromax camera (Princeton Instruments, Trenton, NJ) commanded through the Axiovision software of the Zeiss

microscope or the Metamorph 3.0 software (Universal Imaging, West Chester, PA). A 20× objective was used. All the experiments were performed at room temperature (23 ± 2°C).

Myelin monolayer measurements

Surface pressure-molecular area compression isotherms of lipid or lipid-protein films were registered in a homemade Langmuir balance (20). The surface pressure and surface potential (measured with an air ionizing ^{241}Am electrode and an Ag/AgCl reference electrode) were simultaneously registered. Absence of surface active impurities in the subphase or in the spreading solvents was ascertained by the invariance of surface potential and surface pressure under compression. The compression rate was <10 Å^2 mol^{-1} min^{-1}. Monolayers were spread from their chloroform: methanol solutions in an 80-ml Teflon-coated compartment filled with TRIS-Ca^{+2} buffer PH 7.4 (10 mM Tris, 100 mM NaCl, 20 mM $CaCl_2$). Aliquots of 10–15 nmol of lipids (in no more than 30 μl) were spread reaching initial surface pressures not above 1 mN/m. The solvent was allowed to fully evaporate before beginning compression.

The monolayer phase transitions were detected from the maximum and the transition midpoint from the minimum, of the surface compressibility modulus K ($K = Cs^{-1}$, where Cs is the compressibility), that represents the in-plane elasticity calculated as follows (32):

$$K = (-A)(dp/dA), \quad (2)$$

being A the average molecular area at each surface pressure (p) value.

Myelin Langmuir-Schaeffer films

Monolayers were transferred onto alkylated glass coverslips through the horizontal contact of the glass with the monolayer and then immersing the coverslip into the aqueous subphase (19,27). Glass coverslips were prepared for the alkylating reaction by consecutive sonication for 5 min first in high-grade acetone and then in Milli-Q water; subsequently they were cleaned by submersion in a piranha solution (30% hydrogen peroxide in sulfuric acid) during an hour at 90°C. To alkylate the glass surface a self-assembled, covalently linked, monolayer of alkyl-silane was formed after submerging the thoroughly cleaned glass coverslips in a 2.5-mM solution of octadecyl trichlorosilane in toluene during 60 min under constant stirring. The reaction was performed in a dry-air glass chamber. The hydrophobicity of the surface was checked based on the contact angle and the free running of a water drop. The Langmuir-Schaeffer films formed were always kept under aqueous solutions to avoid collapse. The transferred monolayers were stable for at least 1 week and immunolabeling procedures were subsequently performed (27). For this, the films were immunolabeled by incubating with primary antibodies that recognize PLP (mouse anti-myelin proteolipid protein; Serotec, Raleigh, NC) and MBP (rat anti-myelin basic protein monoclonal antibody; Chemicon, Temecula, CA), and fluorescent-labeled secondary antibodies.

RESULTS

Effect of PLP and MBP on the surface thermodynamics and topography of myelin lipids

In our approach we do not attempt to mimic or directly extrapolate our results to the natural myelin membrane since the lipid asymmetry of the natural bilayer membrane is lost when spread as a monolayer; nevertheless, with our system, the effect of myelin proteins on the thermodynamics and topography of the lipid interface, can be explored in films containing essentially all the compositional complexity of the whole natural membrane, under continuously known packing conditions.

In a previous article, and using a different experimental approach, we suggested that PLP is necessary for the induction of the fractal phase since the surface pattern of protein-free myelin lipid films is mostly homogeneous, showing liquid phase coexistence only up to very low surface pressures (see *insets* in Fig. 1, *B* and *C*) (28); the surface pattern of whole myelin monolayers, changing from round-shaped liquid domains at low surface pressures to a viscous fractal phase at high surface pressures is discussed below in Fig. 6. The results are organized by showing first the effect of each individual isolated protein, and then their combined effects on the surface thermodynamics and structuring of the myelin lipids.

It is important to point out that for the analysis of mixtures containing proteins (PLP and MBP) the myelin lipids are treated as one ''pure'' component although they consist of a mixture with >100 different lipids with fixed mol fractions. The compression isotherm for the myelin lipids (Fig. 1 *A*) shows only one collapse point and, as mentioned, remains topographically homogeneous over all the surface pressure range. Deviations from the additivity rule in mixtures of protein (PLP or MBP) and myelin lipids should be interpreted as if the molecular arrangement of the protein or of at least part

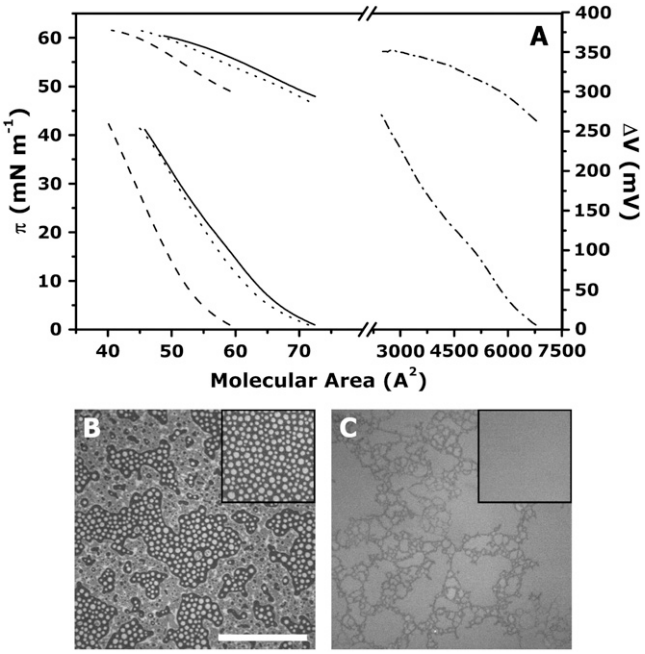

FIGURE 1 Panel *A* shows the surface pressure (*lower curves*), and surface potential (*upper curves*) as a function of the mean molecular area of myelin lipids (*dashed line*), PLP (*dash-dot line*), X_{PLP} 0.00198 mixture (*dotted line*), and the curves, calculated as described in the text, for an ideal X_{PLP} 0.00198 mixture (*solid line*). Panels *B* and *C* are fluorescence microscopy images for films with X_{PLP} 0.00120 at 0.6 mN m^{-1} (*B*) and 30 mN m^{-1} (*C*). The monolayer in panel *B* is doped with Rho-egg PE fluorescent probe. Instead, the film in panel *C* has NBD-DPPE as a probe that markedly improves contrast in these conditions. Insets correspond to fluorescence images of protein-free myelin lipids monolayers at 0.2 mN m^{-1} (*B*) and 30 mN m^{-1} (*C*). The scale bar corresponds to 150 μm.

of the lipids, change compared to the packing of the pure protein or the protein-free myelin lipid films, respectively.

Folch-Lees proteolipid protein

Fig. 1 *A* shows the variation of surface pressure and surface potential as a function of the mean molecular area of myelin lipids, PLP, and a mixture with $X_{PLP}0.00198$ (X being the mol fraction). For comparison, we also show the ideal compression isotherms for the $X_{PLP}0.00198$ mixture calculated by considering a linear contribution of the individual components in the mixed film:

$$(A_M = A_L X_L + A_{PLP} X_{PLP})_\pi \quad (3)$$

$$(\Delta V_M = (\Delta V_L A_L X_L + \Delta V_{PLP} A_{PLP} X_{PLP})/A_M)_\pi, \quad (4)$$

where A_M and ΔV_M are the calculated mean molecular area and mean surface potential of the $X_{PLP}0.00198$ mixed film. A_L, A_{PLP} are the mean molecular areas and ΔV_L, ΔV_{PLP} are the mean surface potentials of films of myelin lipids and of pure PLP. X_L and X_{PLP} are the myelin lipids and PLP mol fractions in the $X_{PLP}0.00198$ mixed film.

In homogeneous mixtures, the most frequent situation is that the mean surface parameters will deviate from the additivity rule as the molecular packing and orientation would likely differ from the single components due to interactions among them. Nevertheless, ideal mixtures with no deviations could also occur. For PLP-myelin lipid mixtures, both independent mean surface parameters change almost additively with composition for the $X_{PLP}0.00198$ mixture (Fig. 1 *A*), and the same behavior was observed for other mol fractions (results not shown). However, the pressure-induced reorganization of PLP, beginning at 11 mN m^{-1}, is no longer observed when mixed with myelin lipids, and the mean molecular area deviations (nearly always below 3%) become maximum at 15 mN m^{-1} in close correspondence to the PLP reorganization range. The fluorescence microscopy (Fig. 1, *B* and *C*) directly reveals that when PLP is added to myelin lipids it induces the lateral segregation of a fractal-like phase, confirming previous results (28). The two-phase coexistence present in the protein-free myelin lipids film at low surface pressures (see *inset* in Fig. 1 *B*) remains and its surface pressure of mixing is not modified by the presence of PLP. The round liquid domains merge at surface pressures below 1 mN m^{-1}, similar to the protein-free lipid mixture; however, the fully homogeneous pattern observed for the pure lipids at higher surface pressures (*inset* in Fig. 1 *C*) is replaced by a fractal-like structure (Fig. 1 *C*).

Myelin basic protein

Graphs *A–D* in Fig. 2 show the dependence on the MBP mol fraction, at 5 and 40 mN m^{-1}, of the mean molecular area and mean surface potential/molecule in mixed MBP-myelin lipids films. Two different features are readily recognized depending on the surface pressure. At 5 mN m^{-1}, MBP contributes rather additively to the mean molecular area and mean surface potential per molecule as expected from either a nonmixing or an ideal mixing of components (Fig. 2, *A* and *B*). However, at 40 mN m^{-1} MBP no longer contributes to any of those mean surface parameters (Fig. 2, *C* and *D*), suggesting the exclusion of the protein from the film (this may correspond to the collapse of pure MBP beginning at 10 mN m^{-1}). The progress of the reorganization as a function of the surface pressure is shown in Fig. 2 *E*. Here, the actual mean molecular area of a myelin lipid film with X_{MBP} 0.0092 was converted to relative areas taking two different theoretical limiting reference states. The first limit is a mixed film with MBP incorporated in the interface and contributing additively to the mean molecular area (see scheme *f* in Fig. 2). For a quantitative estimation of the latter over the whole compression range it was assumed that the protein remains integrated to the interface after its collapse, conserving its limiting mean cross-sectional area, and contributing proportionally to the mean molecular area in the mixed film. The second limit corresponds to a film of myelin lipids with MBP excluded from the interface (see scheme *g* in Fig. 2). The transition from one limiting reference state of surface organization to the other occurs over a surface pressure range beginning at ~16 mN m^{-1} (Fig. 2 *E*).

The surface pressure versus MBP mol fraction phase diagram for films of MBP with myelin lipids is shown in Fig. 3 *A*. Notice that this is a pseudobinary phase diagram since the myelin lipids actually consist of a mixture; the mol fraction of MBP is relative to the total components. Within this context, ''myelin lipids'' imply fixed relative proportions of the lipid components in such a way that when MBP mol fraction is known, all other mol fractions become fixed. The phase diagram was elaborated on data from fluorescence microscopy (and BAM) and the analysis of compression isotherms of mixed and pure monolayers. The isotherms of mixtures of MBP and myelin lipids show a discontinuity in the slope that is well detected by a local maximum and a local minimum of the in-plane elasticity (compressibility modulus, K). The first maximum, indicating the beginning of reorganization, is shown for pure MBP and for mixed monolayers (Fig. 3 *A*, *open circles*); it remains essentially invariable with changes of the proportion of MBP. The first minimum, pointing to the surface pressure midpoint of the transition (π_m), is only shown for MBP-myelin lipids films (Fig. 3 *A*, *open diamond*) because films of pure MBP are fully collapsed at that surface pressure. The π_m remains constant at high MBP mol fractions but diminishes near X_{MBP} 0.0092 approaching the onset of the transition. On the other hand, a second maximum in K (Fig. 3 *A*, *open down-triangle*), indicating the beginning of collapse, is independent on the addition of MBP compared to that of protein-free films up to X_{MBP} 0.0092; above that, and coincidental with the first reorganization point in the isotherm, it increases and then remains constant.

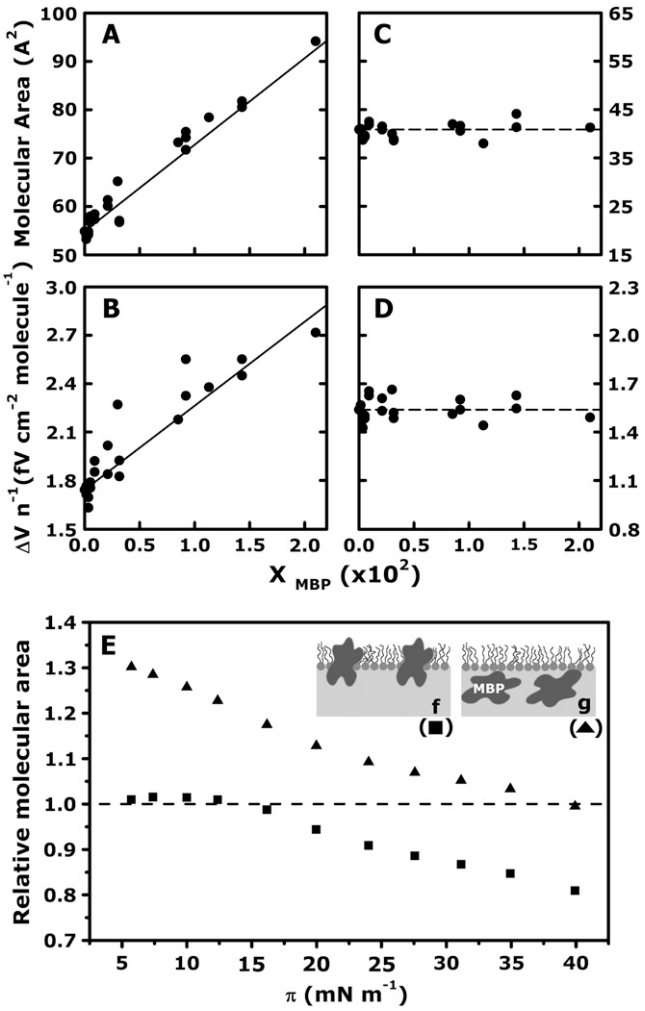

FIGURE 2 Panels *A–D* show the mean molecular area (*A* and *C*) and mean surface potential per molecule (*B* and *D*) at 5 mN m^{-1} (*A* and *B*) and 40 mN m^{-1} (*C* and *D*) as a function of the MBP mol fraction for films of MBP and myelin lipids. The continuous lines in panels *A* and *B* represent the mean values of each parameter for the ideal (additive) contribution of both components in the mixture. The dashed lines in panels *C* and *D* indicate the mean values for each parameter corresponding solely to the myelin lipids. Panel *E* shows the mean molecular area of a X_{MBP} 0.0092 mixed film expressed as a ratio relative to two limiting reference states. The first, (scheme *f*, ■), considers that MBP is included in the myelin lipid film contributing additively to the mean molecular area. The protein is considered to remain in the film even after reaching its collapse surface pressure and conserving the same molecular area at collapse (limiting molecular area). The second reference state (scheme *g*, ▲), considers that MBP is excluded from the film over the whole surface pressure range, and the mean molecular area is that of the myelin lipids. A value of 1 for the relative mean molecular area indicates that the actual area of the film matches with the mean molecular area of the respective reference state (*dashed horizontal line*).

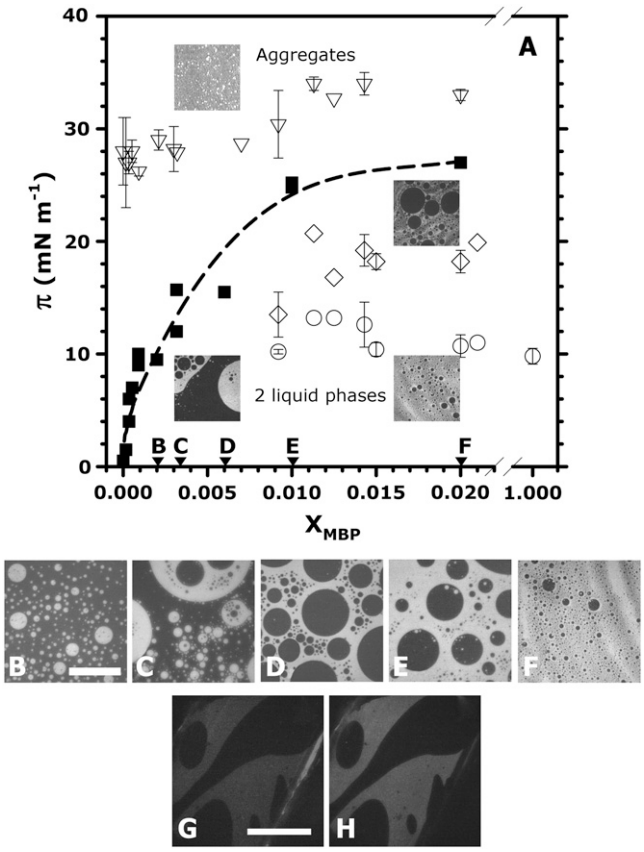

FIGURE 3 Panel *A* shows the surface pressure-MBP mol fraction pseudobinary phase diagram of MBP-myelin lipids monolayers. Values obtained from the isotherm analysis correspond to the transitions evidenced by discontinuities in the surface pressure-molecular area compression isotherms detected as a local maximum (○) and a local minimum (◇) in the compressibility modulus. The beginning of collapse, detected as a local maximum in the isotherms is also indicated (▽). The limits for the two-liquid-phase coexistence were determined by fluorescence microscopy as the surface pressure point where domains first appear after expansion of an initially homogeneous film (■). The dashed line represents the best fit to those values. Representative fluorescence images in the two-liquid-phase coexistence region were included in panel *A*. Images are shown for films with X_{MBP} 0.0200 at 5.8 mN m^{-1} (*right lower image*) and 20.5 mN m^{-1} (*right upper image*) and for a film with X_{MBP} 0.0032 at 5.0 mN m^{-1} (*left image below* the *dashed line*). A BAM image of a film with X_{MBP} 0.0032 at 34 mN m^{-1} is also included to illustrate the region of the phase diagram where aggregates are formed (*left image above* the *dashed line*). Panels outside the phase diagram (*B–F*) are fluorescence microscopy images corresponding to myelin lipids-MBP films, at 3.0 mN m^{-1}, containing 0.0020 (*B*), 0.0032 (*C*), 0.0060 (*D*), 0.0100 (*E*), and 0.0200 (*F*) MBP mol fraction (the corresponding mol fractions are indicated with *arrows* in the abscissa of panel *A*). Panels *G* and *H* are fluorescence microscopy images of the same area of a Langmuir-Schaeffer film with X_{MBP} 0.0032 transferred at 10 mN m^{-1}. The label corresponding to the anti-MBP (*H*) colocalizes with the fluorescent probe, Rho-egg PE (*G*). Scale bar represents 150 μm in fluorescence images and the side length of the BAM image is 1083 μm.

The results from fluorescence microscopy show that MBP mixed with myelin lipids induces the coexistence of two phases at surface pressures above 1 mN m^{-1} in the otherwise homogeneous surface organization of the protein-free lipids (Fig. 3, *B–F*). As the proportion of MBP increases, the probe enriched phase becomes larger in area suggesting that the protein partitions into that phase as further confirmed by the labeling with anti-MBP on the Langmuir-Schaeffer transferred monolayers (Fig. 3, *G* and *H*). Further measurements of the area covered by the fluorescent phase and the area

occupied by MBP, calculated from its compression isotherm, indicate that MBP should be associated with lipids forming a protein-lipid phase (see Appendix). The segregated domains merge under compression but the stability gap of the two-phase state is increased by higher proportions of MBP in the film up to a plateau (Fig. 3 *A*, *solid squares* and *dashed line*). Both coexisting phases are liquid, with mostly circular deformable domains, and boundaries that fluctuate as a result of thermal motion, all indicative of relaxed line tension. This feature, together with a high rate of events of lateral merging, confers a conspicuous dynamics to the surface pattern that changes under the compression from homogeneously sized, small and numerous domains, to large and more dispersed ones. The electrostatic repulsive barriers that need to be overcome to bring domains into contact and merging do not seem to be above the order of the thermal energy for this system.

When the percentage of area of fluorescent phase is analyzed as a function of surface pressure we found one or two different behaviors depending on the MBP proportion (Fig. 4 *A*). For films with low MBP mol fractions (X_{MBP} 0.0060 and below) there is a monotonic decrease of fluorescent phase that finally disappears by merging (Fig. 4 *A*, *solid triangles*). For higher MBP mol fractions the area occupied by the fluorescent phase first decreases with a slight slope, a behavior analogous to films with low MBP mol fractions, but this is followed by a second regime with higher slope that is maintained until the phases fully merge (Fig. 4 *A*, *solid circles and crosses*). The surface area of fluorescent phase markedly decreases until it becomes reduced to small regions around the boundary of fluorescence-depleted domains (Fig. 4 *D*). The surface pressure point where the second regime begins (Fig. 4 *A*, *arrow*) is close to the minimum of the in-plane elasticity (Fig. 3 *A, open diamond*) and coincides with the pressure point for monolayer exclusion of MBP (Fig. 2 *E*). This second regime appears when the region where MBP is stably included in the interface is below the stability gap for two-phase coexistence. Then, disappearance of the fluorescent phase becomes dependent on the exclusion of MBP from the interface and the regime of surface dynamics changes.

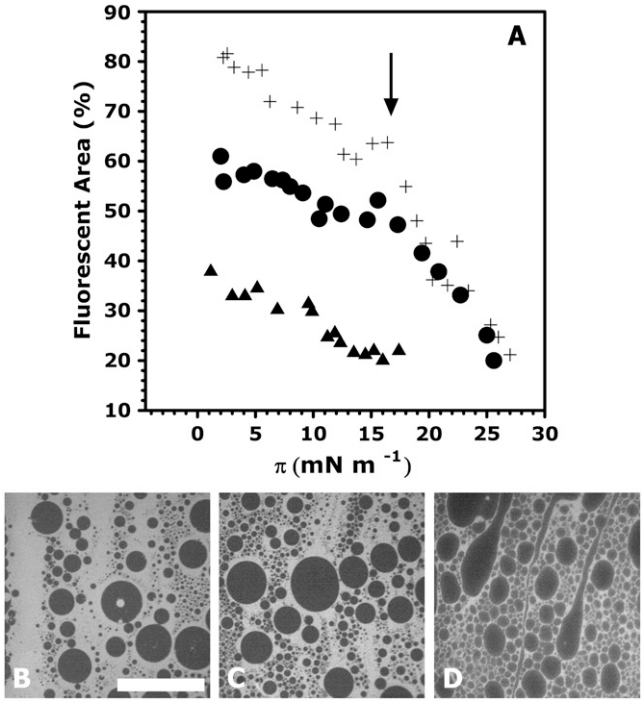

FIGURE 4 Panel *A* shows the percent of fluorescent phase area, measured from fluorescence microscopy images as a function of surface pressure for films with mol fractions of MBP of 0.0032 (▲), 0.0100 (●), and 0.0200 (+). The vertical arrow approximately indicates the surface pressure at which the change in behavior takes place. Panels *B–D* show fluorescence microscopy images of films with X_{MBP} 0.0100 at 5.8 mN m^{-1} (*B*), 15.6 mN m^{-1} (*C*), and 25.0 mN m^{-1} (*D*). The scale bar represents 150 μm.

MBP relocation within the interface

After MBP is excluded from the surface film it could either desorb from the interface or adopt a stable, or unstable (but kinetically trapped), organization adjacent to the monolayer. The localization of MBP was studied by Brewster angle microscopy (BAM), a technique that can distinguish variations of optical thickness among different regions of the same film or within a particular region as a function of time because relative reflectance values are proportional to the interfacial thickness ($I \sim t^2$, where I is the relative reflectance and t is thickness) (31). BAM has been previously used to describe the variations of optical thickness of interfaces formed with glycosphingolipids with oligosaccharide chains of different length (31) and to detect the formation of protein aggregates in lipid films at the air-water interfaces (33,34). Fig. 5, *A–C*, shows the surface topography of a film with X_{MBP} 0.0100 at different surface pressures as observed by BAM. After the low pressure surface pattern disorganizes new structures are formed with time that can be clearly visualized as brilliant spots (Fig. 5 *C*). These were also observed in films with lower and higher MBP mol fractions (i.e., X_{MBP} 0.0032 and X_{MBP} 0.0200). The reflectance levels were quantified along the compression isotherms of the films and the results are shown in Fig. 5 *D* for X_{MBP} 0.0100. The MBP-containing and MBP-free phases present at low surface pressures were identified and separately quantified by comparing BAM and fluorescence images of the same field. The MBP-free lipid phase shows an almost invariant reflectance level as a function of surface pressure that is similar to that observed for myelin lipid monolayers (compare Fig. 5 *D*, *solid circles* with *inset* (*solid circles*)). As already discussed in a previous article (28), the myelin lipid fraction contains a high percentage of cholesterol (40%) and shows a rather condensed isotherm, with a limiting close packing at 41 $Å^2$ and only a small lateral and transverse reorganization. By contrast, the MBP-containing phase largely increases its reflectance during compression (Fig. 5 *D*, *solid squares*). The range of values over which the increment of reflectance

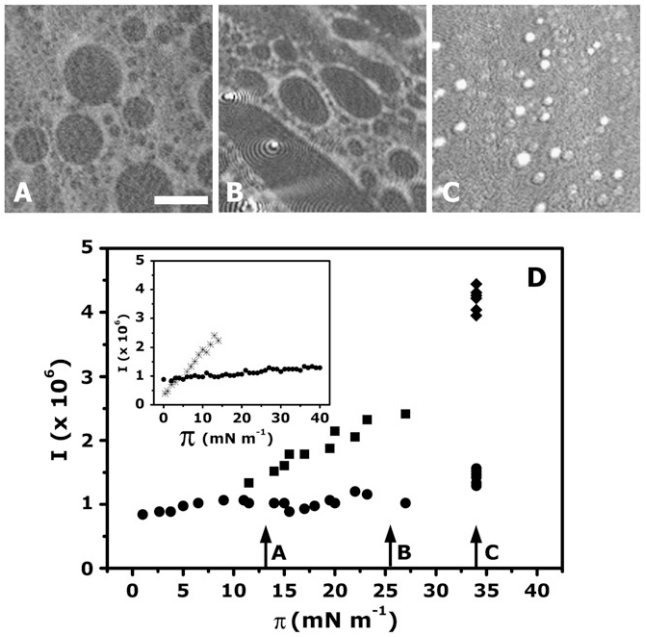

FIGURE 5 Panels *A–C* are BAM images of a myelin lipids film with X_{MBP} 0.0100 at 12.9 mN m^{-1} (*A*), 25.2 mN m^{-1} (*B*), and 34.0 mN m^{-1} (*C*). BAM images are shown at 1/50 shutter speed to improve contrast. Panel *D* shows the relative reflectance levels as a function of surface pressure for a film with X_{MBP} 0.0100. The relative reflectance measured by BAM of MBP-containing fluorescent phase (■) and the MBP-free nonfluorescent phase (●) were separately quantified at low surface pressures by comparison with fluorescence microscopy images of the same field. The reflectance levels of the high pressure domains are also indicated (♦). The relative reflectance values were computed from images taken with 1/500 shutter speed (our BAM was calibrated under those conditions; see Materials and Methods section). Arrows *A*, *B*, and *C* are indicative of the surface pressures corresponding to panels *A–C*. The inset shows the relative reflectance levels as a function of surface pressure for pure films of MBP (*) and myelin lipids (●). The scale bar represents 285 μm.

levels occurs is similar to that of pure films of MBP up to collapse (compare Fig. 5 *D*, *solid squares*, and *inset* (*stars*)). The high pressure bright domains (measured at 34 mN m^{-1}) seemingly represent a jump in reflectance after the monotonic increase (Fig. 5 *D*, *solid diamond*). The reflectance of these structures must involve new arrangements requiring the presence of both myelin lipids and MBP because none of the individual components achieves those reflectance values. Results strongly suggest that the protein remains adjacent to the interface, forming aggregated structures at surface pressures in the range of average pressures usually assumed for membranes (35). When the film is expanded, the MBP-induced low pressure pattern of round domains self-organizes again (not shown) indicating that the alternation among both topographic arrangements represents a reversible protein reorganization along the perpendicular direction to the interface, with MBP remaining associated to the monolayer. In the region above the two liquid phase coexistence (Fig. 3 *A*) MBP becomes aggregated adjacent to the monolayer of myelin lipids. Moreover, this is an equilibrium organization that can be also reached by adsorption of MBP from the subphase (see below).

Combined effects of PLP and MBP on myelin lipids

Apart from the effect of each of the myelin proteins on the surface pattern organization, we aimed at recognizing how both proteins may interact and if their separate effects could combine to reconstitute the surface pattern of the monolayer formed by whole myelin (Fig. 6, *A* and *B*).

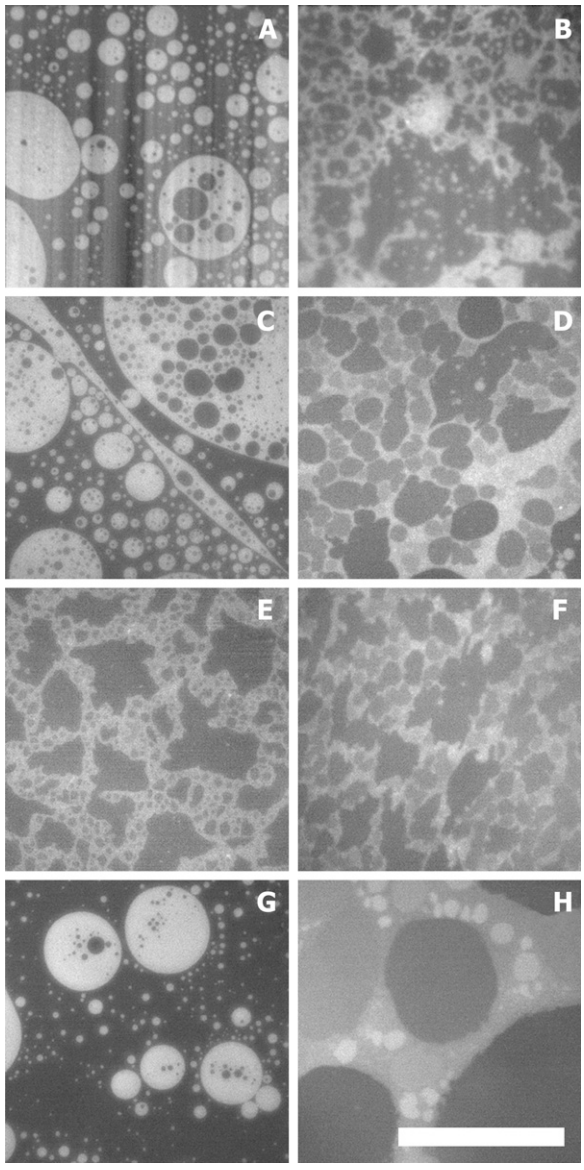

FIGURE 6 Fluorescence microscopy images of whole myelin (*A* and *B*) and premixed MBP-PLP-myelin lipids monolayers (*C–H*) at 3.0 mN m^{-1} (*A*, *C*, *E*, and *G*) and 35 mN m^{-1} (*B*, *D*, *F*, and *H*), with variable mol fractions of PLP ($X_{PLP} = 0.00180$ for *C–F* and $X_{PLP} = 0.00050$ for *G* and *H*) and MBP ($X_{MBP} = 0.0032$ for *C*, *D*, *G*, and *H* and $X_{MBP} = 0.0005$ for *E* and *F*). The scale bar represents 200 μm.

We observed the pattern of mixed films in which the relative protein proportions were varied (Fig. 6, *C–H*). As stated before, when only PLP is included in the monolayers with myelin lipids, it induces the organization of segregated domains with a fractal-like appearance and the coexistence with liquid round-shaped domains is maintained only up to 1 mN m^{-1} (Fig. 1, *B* and *C*). On the other hand, when only MBP is present in the myelin lipid film it stabilizes the coexistence of two liquid phases (Fig. 3, *B–F*), whose surface pressure for merging depends on the MBP proportions, with absence of fractal pattern at higher surface pressures and with the protein becoming excluded to a plane adjacent to the monolayer (Fig. 5 *C*). When both MBP and PLP are present in films with the total myelin lipid fraction, in the same proportions as in the whole myelin membrane, the pattern becomes very similar to that exhibited by the whole myelin monolayer (compare Fig. 6, *C* and *D*, with Fig. 6, *A* and *B*). Moreover, in films formed with a premixture of MBP, PLP, and myelin lipids (at 12.8 and 35 mN m^{-1}) labeling to both proteins always colocalizes in the same phase, similar to what was found in the monolayer formed with whole myelin (27) (Fig. 7). If the proportion of MBP is decreased, the general pattern becomes dominated by the PLP effect evidenced by the acquisition of the general fractal appearance. In the range of low surface pressures, the thoroughly connected domains have rather rounded relaxed boundaries that turn into rigid borders at high surface pressures (Fig. 6, *E–F*). Conversely, if the proportion of PLP is decreased, the pattern is reverted to round-shaped liquid domains at low surface pressures and, at high surface pressures, clusters with a fractal-like aspect appear (Fig. 6, *G–H*). Interestingly then, the organization of the probe enriched phase at low pressures, as fractal-like or as round boundary domains, depends on the relative proportions of PLP and MBP. At high pressures, when MBP is excluded from the film, a fractal-like pattern always appears if PLP is present. Also, the proportion of the fluorescent phase at low surface pressures coincides with the sum of the amount of fluorescent phase induced by MBP (for each mol fraction) and PLP. This reinforces the colocalization of both proteins.

We have further inquired if in whole myelin monolayers, apart from their colocalization (Fig. 7), both proteins may mutually influence their surface organization. In Fig. 8 *A* we show that in mixtures of myelin lipids and both proteins, MBP still reorganizes by escaping from the interface with a surface pressure dependence very similar to that observed in the absence of PLP (see Fig. 2 *E*). Thus, PLP is not capable of retaining MBP inserted in the monolayer at relatively high surface pressures; nevertheless, MBP still remains associated to the interface, as detected by immunolabeling (Fig. 7 *H*), but in the subsurface adjacent to the monolayer. In mixed films of PLP and MBP both components contribute additively to the mean molecular area (Fig. 8 *B*) and, in mixed monolayers with both proteins and myelin lipids, deviations from the ideal behavior at low surface pressures (below MBP collapse) were never detected. This can be deduced from Fig. 8 *A* and was also ascertained for other protein proportions (not shown).

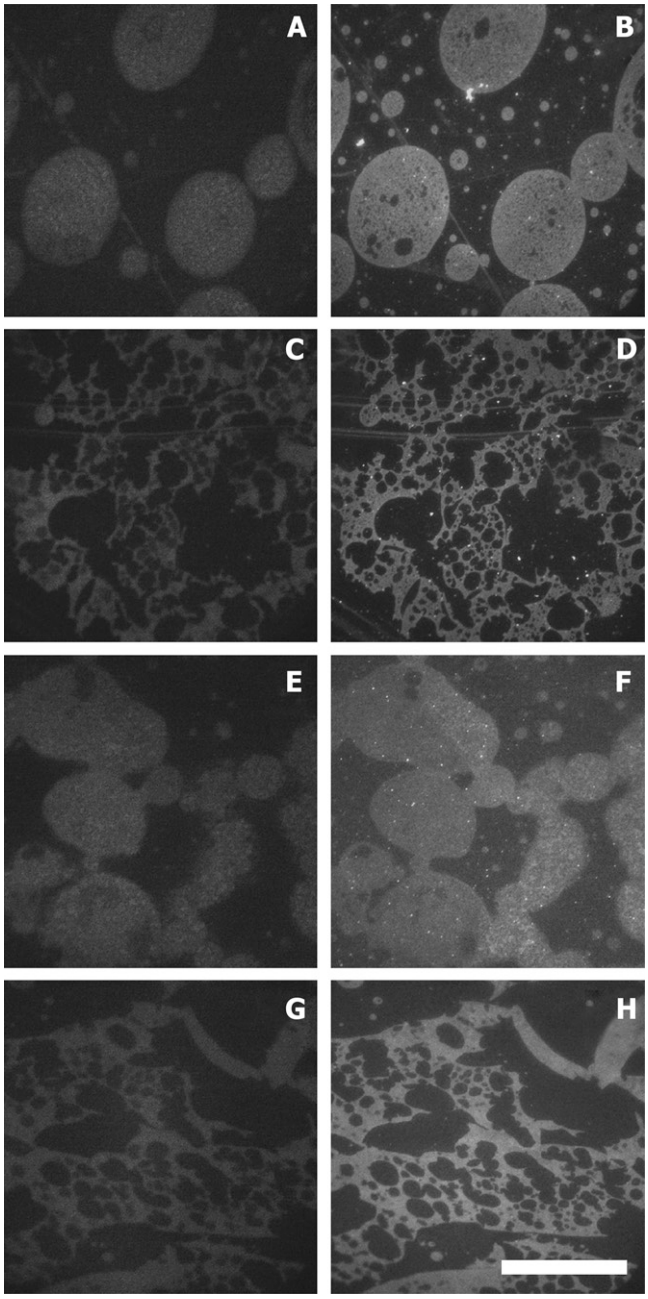

FIGURE 7 Fluorescence microscopy images of Langmuir-Schaeffer films of premixed myelin lipids PLP (X_{PLP} 0.00180)-MBP (X_{MBP} 0.0032) at 12.8 mN m^{-1} (*A*, *B*, *E*, and *F*) and 35 mN m^{-1} (*C*, *D*, *G*, and *H*). The label for the fluorescent probe Rho-egg PE (*A*, *C*, *E*, and *G*) and the anti-PLP (*B* and *D*) or anti-MBP (*F* and *H*) are shown for the same field areas. The scale bar represents 150 μm.

We also measured the penetration, as an increase of surface pressure, of MBP into monolayers of myelin lipids, pure PLP, and in mixed PLP-myelin lipids films (X_{PLP} 0.00180,

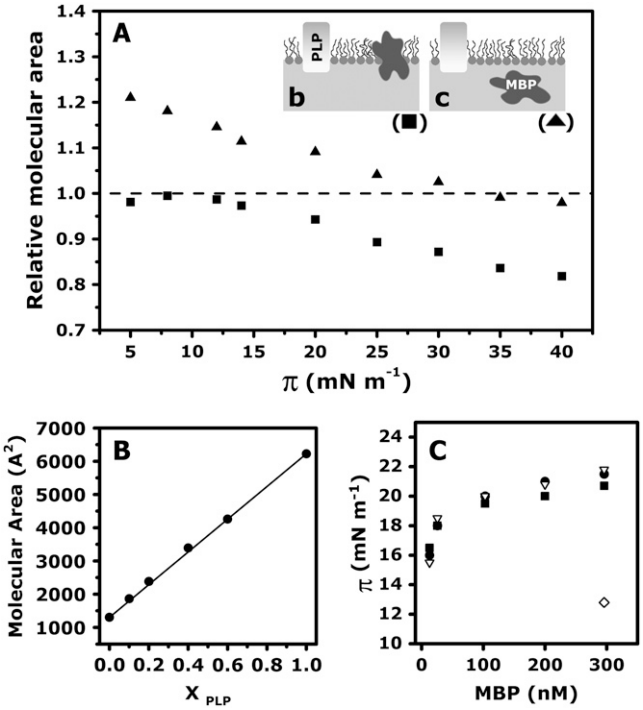

FIGURE 8 Panel *A* shows the mean molecular area of a MBP-PLP-myelin lipids films (X_{MBP} 0.0090, X_{PLP} 0.00292) as a function of surface pressure, expressed as a ratio relative to two limiting reference states. The first considers that all the components are included in the film and contribute additively to the mean molecular area (scheme *b*, ■); the MBP is considered to remain in the film after its collapse occupying its limiting molecular area. The second reference state (scheme *c*, ▲) considers that MBP is excluded from the film and the mean molecular area is that of an ideal PLP-myelin lipids film (X_{PLP} 0.00292). A relative mean molecular area of 1 indicates that the actual area of the film matches with the mean molecular area of the respective reference state (*dashed horizontal line*). Panel *B* shows the mean molecular area as a function of the PLP mol fraction of MBP-PLP mixed monolayers at 8.0 mN m^{-1}. The continuous line represents the mean molecular area resultant from a lineal contribution of both components in the mixture (ideal mean molecular area). Panel *C* shows the final surface pressure of films of PLP (■), myelin lipids (●), and PLP-myelin lipids (X_{PLP} 0.00180, ▽) initially at 12.5 mN m^{-1}, after the adsorption of MBP solubilized in the subphase at the indicated concentrations. The surface pressure reached after the adsorption of MBP at the clean air-water interface is also indicated (◇).

the proportion in natural myelin) initially organized at 12.5 mN m^{-1} (the equilibrium surface pressure of MBP at the air-water interface). If there were favorable interactions of MBP and PLP that could stabilize the former in the interface, then the presence of PLP should lead to increases of surface pressure (due to penetration of MBP) above that obtained in PLP-free myelin lipid monolayers and this was not observed (Fig. 8 *C*). In fact, the surface pressure change after the adsorption of MBP (from 25 to 300 nM in the subphase) to any of the interfaces is quite similar.

The surface properties of one component (i.e., packing, stability) should change due to the presence of another if new interactions occur at the interface. Our results show that none of the surface properties measured for a protein are influenced by the presence of the other protein at the interface. They occupy the same molecular areas; MBP experiences the same surface pressure-dependent rearrangement and produces the same surface pressure increase after adsorption, in the presence or absence of PLP in the myelin lipid interface. These results as a whole suggest no interaction among both proteins.

Equilibrium and nonequilibrium patterns

It would be expected that if a surface organization represents a relatively stable equilibrium condition it should be attainable from different initial situations. We have explored if similar patterns could be obtained from the adsorption of MBP from the subphase and in premixed films. Fig. 9, *C* and *D*, shows the adsorption of MBP to a film of myelin lipids initially at 28.5 mN m^{-1} as detected by BAM. After the injection of MBP in the subphase, the originally homogeneous interface (Fig. 9 *C*) becomes covered with round bright domains without changes of the surface pressure (Fig. 9 *D*). The reflectance level, shown in the inset of Fig. 9 *D*, is similar to that of domains formed in premixed MBP-myelin lipids films at 34 mN m^{-1} (Fig. 5 *D*) and no variations occur in the reflectance of the background (*inset*, Fig. 9, *C* and *D*). The adsorption of MBP to a mixed film of PLP and myelin lipids (X_{PLP} 0.00120) initially at 28 mN m^{-1} is shown in Fig. 9, *I–L*. The images reveal no clear pattern at first (Fig. 9 *I*) but after MBP is added to the subphase, the contrast gradually increases with time and a fractal-like pattern becomes clearly noticeable (Fig. 9, *J–L*). This change is also evident in the surface plots of the images corresponding to the film before MBP injection (Fig. 9 *M*) and after maximum contrast was reached (Fig. 9 *P*).The effect of MBP is primarily on the PLP-induced fractal-like structure that increases its thickness, and only a few round-shaped aggregates are also formed (not shown). Another indication that the fractal-like phase changes its properties after MBP adsorption is the variation of the Rho-egg PE fluorescent probe partition. As shown in Fig. 9, *N* and *O*, only after the adsorption of MBP the fractal becomes visible (the *inset* in Fig. 9 *N* is included as a control that the fractal is always present because it can be detected with another probe, NBD-DPPE). Again, no surface pressure variation is produced after MBP adsorption.

At ~12 mN m^{-1} the adsorption of MBP to films of protein-free myelin lipids induces, concomitantly with a surface pressure increase, the pattern of round-shaped liquid domains that MBP also induces in premixed MBP-myelin lipid mixed monolayers (Fig. 9, *A–B*). Finally, when MBP adsorbs to a PLP-myelin lipid film (X_{PLP} 0.00120) initially at 12.8 mN m^{-1}, a liquid phase is induced as circular domains and around the fractal-like phase. The resultant surface pattern closely resembles that of whole myelin monolayers and premixed PLP-MBP-myelin lipids films (compare Fig. 9 *H* with Fig. 6, *A* and *C*). It is interesting that, as MBP adsorbs to

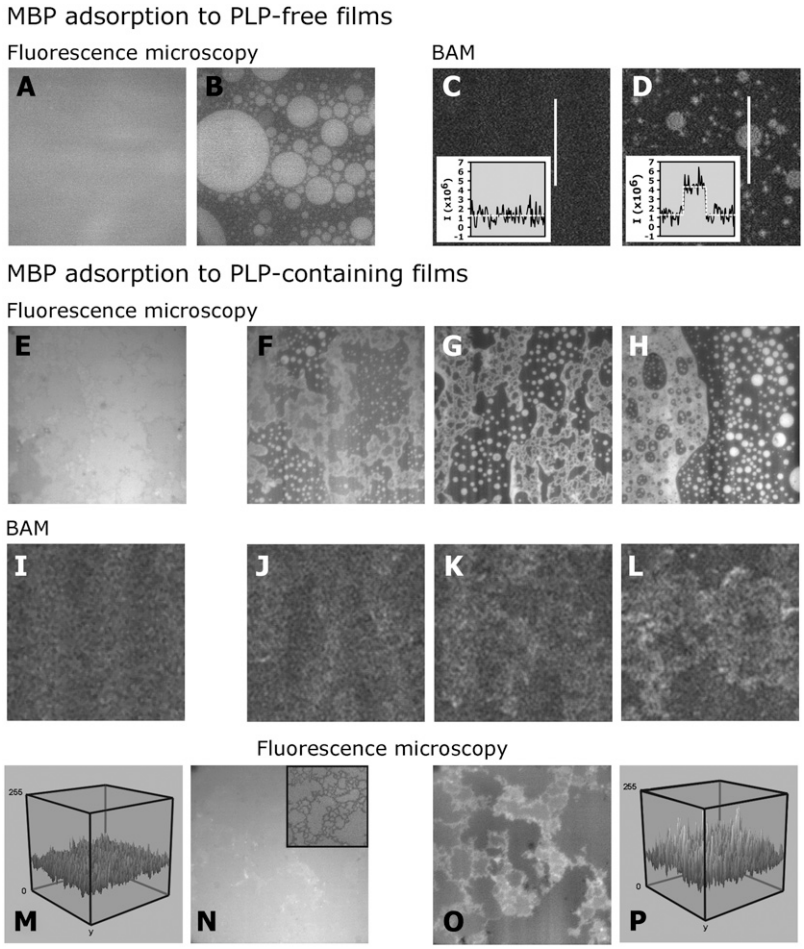

FIGURE 9 Fluorescence microscopy (*A*, *B*, *E–H*, *N*, *O*) and BAM (*C*, *D*, *I–L*) images of myelin lipids (*A–D*) or PLP-myelin lipids films (X_{PLP} 0.00120) (*E–L*, *N*, *O*) before (*A*, *C*, *E*, *I*, *N*) and after (*B*, *D*, *F–H*, *J–L*, *O*) the injection of MBP in the subphase (100 nM). Myelin lipids monolayers were set initially at 12.0 mN m^{-1} (*A*) and 28.0 mN m^{-1} (*C*), and surface pressure was 17.5 mN m^{-1} 18 min after MBP injection (*B*) and 28.0 mN m^{-1} 110 min after MBP injection (*D*). PLP-myelin lipids monolayers were initially at 12.5 mN m^{-1} (*E*) or 28.0 mN m^{-1} (*I*, *N*). Surface pressure was 16.5 mN m^{-1} (*F*) and 17.5 mN m^{-1} (*G* and *H*), after 13 (*F*), 36 (*G*), and 37 (*H*) min from the injection of MBP. Surface pressure remained at 28.0 mN m^{-1} at 16 (*J*, *O*), 54 (*K*), and 120 (*L*) min after MBP injection. All BAM images were taken with 1/500 shutter speed and are shown without further processing in panels *C* and *D*. In panels *I–L*, the grayscale level range ($GL \in [0, 255]$) was equally normalized ($GL \in [0, 140]$) to improve contrast. The insets in panels *C* and *D* are line plots of the reflectance as a function of the position along the vertical white lines. Panels *M* and *P* are surface plots of the gray level intensity as a function of *x* and *y* coordinates corresponding to images *I* (surface plot *M*) and *L* (surface plot *P*). The inset in panel *N* corresponds to a film with X_{PLP} 0.00120 at 30 mN m^{-1} doped with 1 mol % of NBP-DPPE, instead of 0.8 mol % of Rho-egg PE, which is the probe used otherwise (*A*, *B*, *E–H*, *N*, *O*). The scale bar in BAM images represents 350 μm, which is the side length of the fluorescence microscopy images.

the interface, intermediate states are self-organized, exhibiting a marked similarity with the pattern of films with high ratios of PLP/MBP (compare Fig. 9 *G* with Fig. 6 *E*).

In summary, the PLP segregates as a fractal-like structure that represents an organization resulting from an out-of-equilibrium process (26). By contrast, the MBP-dependent organization appears to be the result of a near-equilibrium process because it can be reached from completely different initial situations.

DISCUSSION

Recent results on monolayers prepared from pulmonary surfactant conclude that the lateral structure in this system seemingly depends on the presence of cholesterol and not on the surfactant proteins (22,23). On the other hand, our studies provide an insight at the molecular level on the capacity of the two major myelin proteins to induce reorganization of the total lipid components into the complex surface structuring of whole myelin monolayers. In myelin monolayers, both MBP and PLP, individually and in conjunction, acquire an organization where they become segregated from all or part of the myelin lipids (27). Depending on the surface pressure, MBP adopts two clearly distinct surface organizations that imply different interactions with the lipids. Both organizations are rather stable equilibrium conditions since their surface topography can be reached from different initial situations: in premixed spread films and by adsorption of MBP from the subphase; the last condition rules out that the presence of MBP at the interface could be due to the existence of kinetic barriers that impair the desorption of the protein. The transition among both states is surface pressure dependent and the arrangement acquired at high surface pressure is reminiscent of that described in bilayers and natural myelin membranes. However, due to the thermal energy and depending on the in-plane elasticity (36), the surface pressure undergoes large fluctuations, which in turn suggest that MBP could alternate reversibly between at least two possible organizations. MBP has been described as an extrinsic protein (as it can be removed from the interface with high (1 M NaCl) ionic strengths) localized adjacent to the bilayer, likely stabilized through electrostatic interactions with the lipid polar headgroups (37–39), and there are also evidences for hydrophobic interactions (40). The concept that some segments of MBP could be embedded in the membrane interface was proposed long ago on the basis of

experiments with proteolytic enzymes acting on monolayers (41) and was later supported by various evidences (37,42–44). In the reconstituted monolayers the protein is arranged adjacent to the interface but it does not induce any noticeable deviation from the average molecular area of the lipids, indicating that the interaction is peripheral and the effect of the insertion of protein segments into the lipid interface, if any, is less than the error of area determination regarding monolayer packing. No deviations were observed at high surface pressures in other lipid monolayers such as sulfatide, whereas area contraction occurred in ganglioside films (45); also, some effects derived from MBP penetration in the acyl chain region were observed to vary among different lipids (40). All these data reinforce the concept of MBP as a highly adaptable protein that can adopt different organizations at the interface (46) depending on the interaction with lipids. On the other hand, in the reconstituted monolayers at high surface pressures, MBP is laterally self-interacting forming micron-size aggregates. The state of aggregation is not known in vivo but MBP autoassociates in bulk in the presence of amphiphiles and some effects on vesicle aggregation appear to depend on multiple protein interactions (47).

At low surface pressures, MBP is completely inserted in the monolayer and exerts a different impact on the lateral distribution of lipids actually inducing the segregation of two liquid phases. In films of whole myelin, two liquid phases are also present and MBP becomes segregated from a probe-depleted cholesterol enriched phase (27). This low surface pressure organization of MBP probably requires a more deformable or elastic environment and the protein insertion, coupled to the nonideality of the cholesterol containing lipid mixtures, appears to be enough for inducing phase segregation. In bilayer membranes, the exclusion from cholesterol-enriched phases can act as a mechanism by which proteins induce lipid domains as extensively reviewed recently (17). To get more insight into this MBP-lipid stabilizing interaction, an estimation of the ratio of lipids/MBP molecules was calculated for different MBP proportions, based on direct measurements of the area occupied by the fluorescent phase and the mean molecular area of MBP obtained from its compression isotherm (see Appendix). The number of lipid molecules per MBP at different surface pressures is shown in Fig. 10 for four mol fractions. At lower proportions of MBP, the protein can recruit a larger number of lipid molecules that decrease with the surface pressure. When the mol fraction of MBP increases, the number of lipid molecules recruited by the protein diminishes. Considering the lipid shell surrounding MBP, it could vary from approximately three to four or two to three lateral concentric layers at low or high protein proportions, respectively. These values are fully coincident with early calorimetric studies (44) and with the correlation lengths described for liquid phases (48) that relate to the propagation of a defect into the lipid phase, being MBP the perturbing factor. Moreover, in films with low mol fractions

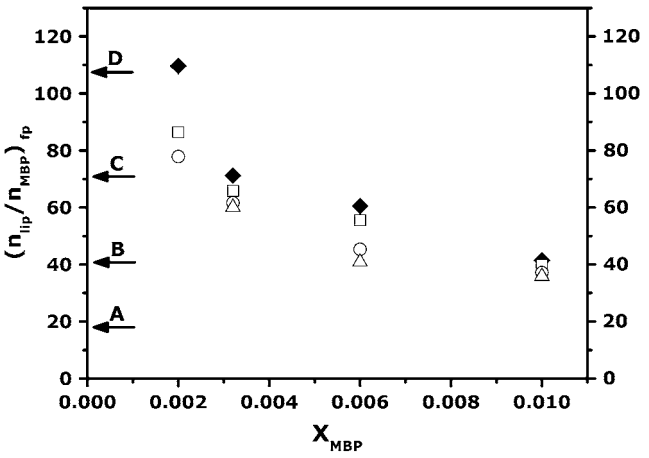

FIGURE 10 Number of lipid molecules per MBP molecule in the fluorescent phase $(n_{lip}/n_{MBP})_{fp}$, calculated as stated in the Appendix, for 2.5 mN m^{-1} (♦), 4.5 mN m^{-1} (□), 8.5 mN m^{-1} (○), and 10.5 mN m^{-1} (△) in films with 0.0020, 0.0032, 0.0060, and 0.0100 MBP mol fractions. The arrows indicate the number of lipid molecules calculated for one (*A*), two (*B*), three (*C*), and four (*D*) layers around each protein molecule.

of MBP it can be seen that, besides the lipids that remain associated to the protein, some fluorescent phase lipids become mixed at a surface pressure $\leq$1 mN m^{-1} (as in protein-free films). The relative proportions of these two populations change in favor of an increase of the protein-associated lipids when the MBP mol fraction increases. This suggests that the effect of MBP on the stability of the phase segregation is mediated by local interactions with certain lipids in the nearest environment and not by a more global and longer range effect.

PLP and MBP colocalization

The interaction of PLP and MBP has been proposed in some myelin models (25), but experimental evidence in simple reconstituted systems has not supported a direct interaction among both proteins (49). Also, under some conditions, all myelin proteins colocalize in natural myelin (50). In the myelin monolayers, MBP and PLP are segregating together in domains but, although no direct measurements of their interaction were made, our observations do not support a mutual perturbation: the mean molecular area of each protein remain unaltered in the presence of the other; MBP experiences the same pressure-dependent reorganization that occurs in the absence of PLP; the surface-pressure increases as a function of MBP concentration in the subphase are not enhanced by the presence of PLP in the myelin lipids film. On the other hand, some other factors must be favoring the concomitant partitioning of MBP with PLP since immunolabeling of both proteins always colocalizes in the same phase domains. This arrangement is likely an equilibrium state because this is also the organization acquired when

MBP is inserted in the interface from the subphase. It was previously suggested that lateral wetting phenomena were occurring at low surface pressures (21). Continuing in that sense now we propose that the structuring factor that nucleates MBP around PLP may simply be the tendency to minimize the lateral interfacial energy among the PLP-containing domains and the cholesterol-enriched liquid phase. Fractal-like structures appear in PLP-myelin lipid mixtures as a result of an out-of-equilibrium coalescence of cluster units having a rather large, nonrelaxed boundary interface (28). On the other hand, PLP has a homogeneous distribution, as ascertained by immunolabeling, in the MBP-induced liquid phase in myelin monolayers (27) contrary to the formation of surface aggregates formed when the protein is incorporated in myelin lipids films. The organization of MBP around the fractal after adsorption from the subphase leads to a long-range restructuring of components and changes the organization of PLP from an aggregated to a dispersed state. The scheme in Fig. 11 summarizes the combined results and provides a possible interpretation.

In cell membranes, some proteins of the cytoskeleton, focal adhesion contacts, pores, and other specialized patches constitute long-lived segregated structures with defined lipid-protein interactions. In our system the final structural dynamics of the whole surface is regulated by coupled equilibrium and out-of-equilibrium processes. We propose that some protein components, behaving as a ''scaffold skeleton'', originated from out-of-equilibrium surface aggregation processes, provide a surface frame that conditions the structuring of the segregated domains. Superimposed on this, the transverse dynamics of other protein component regulated through adsorption/desorption and pressure-dependent extrusion from the interface, finally modulates the surface organization of the interface.

APPENDIX

The following approximation was used to estimate the number of lipid molecules associated to MBP in the fluorescent phase of MBP-myelin lipids films. Based on inmunolabeling, MBP was considered to be all localized in the fluorescent phase (the label intensity of the nonfluorescent phase was similar to the background). Besides, if errors in the proportion of MBP in the fluorescent phase were of the order of 15% (if actually only 85% of the MBP were in the fluorescent phase), this would not alter the conclusions. The total area of the fluorescent phase is assumed to consist of the sum of an area covered by MBP and an area occupied by lipids. The proportion among both areas was first estimated and then converted into a relative number of lipid/MBP molecules as follows.

Since MBP contributes additively with its average molecular area in the mixed film (Fig. 2 *A*), the area of MBP relative to the total area of the film (*AMR*) is simply:

$$AMR = (A_{\mathrm{MBP}}/A_{\mathrm{m}})\,X_{\mathrm{MBP}}, \tag{5}$$

where A_{MBP} is the average molecular area of MBP, A_{m} the average molecular area of the monolayer, and X_{MBP} the MBP mol fraction.

On the other hand, the proportion of area covered by the fluorescent phase (where the MBP is located) is measured directly from fluorescence microscopy images and the area of the lipids in the fluorescent phase relative to the total area of the film is obtained from the subtraction:

$$AL_{\mathrm{fp}}R = AFR - AMR, \tag{6}$$

where $AL_{\mathrm{fp}}R$ is the area of lipids in the fluorescent phase relative to the total area of the monolayer and *AFR* is the area of fluorescent phase relative to the total area of the monolayer (obtained from microscopy images).

Finally, the area occupied by the lipids with respect to the area occupied by MBP in the fluorescent phase is obtained from the ratio:

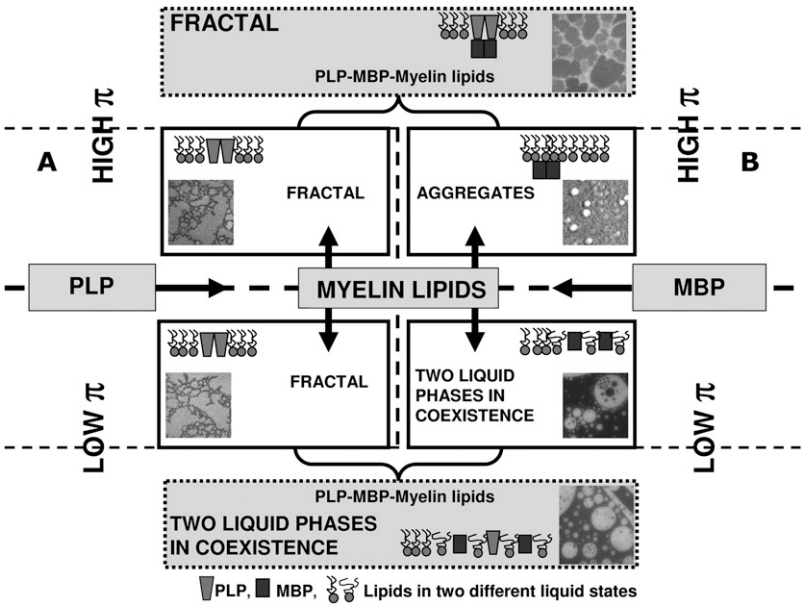

FIGURE 11 Contribution of MBP and PLP to the surface pressure-dependent structuring of myelin monolayers. The figure shows possible arrangements induced by MBP and PLP (see Discussion). The individual effects of PLP and MBP on a myelin lipid film is shown in the central part of the diagram (*between* the *dashed horizontal lines*). The effect of PLP on a MBP-free myelin lipid monolayer, at low and high surface pressures, is represented on the left of the diagram (side *A*) whereas the effect of MBP on a PLP-free myelin lipid monolayer is represented on the right (side *B*). The PLP always organizes as a fractal-like structure when embedded in the myelin lipid phase, independently of the surface pressure. In turn, MBP induces the segregation of two liquid phases at low pressures, while included in the film, and forms aggregates located adjacent to the monolayer at high pressures. The central bottom and upper panels illustrate the combined effects of PLP and MBP, when both proteins are incorporated in a myelin lipid monolayer at low (*bottom panel*) and high (*upper panel*) surface pressure. In these films, PLP mixes in the MBP-induced liquid phase at low pressures but, at high pressures, when MBP is excluded from the film, the PLP becomes surrounded by the myelin lipid phase and structures with a fractal appearance. The images are fluorescence micrographs with the exception of the BAM image corresponding to MBP aggregates formed at high surface pressures in a MBP-myelin lipid film. Images displaying low surface pressure conditions are at 3–5 mN m^{-1} and those displaying high surface pressure conditions are at 30–35 mN m^{-1}.

$$(A_L/A_{MBP})_{fp} = AL_{fp}R/AMR, \quad (7)$$

where $(A_L/A_{MBP})_{fp}$ is the ratio among the area of lipids and the area of MBP in the fluorescent phase.

To estimate the number of lipid molecules per MBP molecule in the fluorescent phase, the mean molecular area of the lipids and MBP are needed. These are assumed to be the mean molecular area of the myelin lipids and MBP obtained from the respective compression isotherms. The relative number of lipids/MBP molecules is calculated as:

$$(n_{lip}/n_{MBP})_{fp} = (A_L/A_{MBP})_{fp}\,(A_{MBP}/A_{lip}), \quad (8)$$

where $(n_{lip}/n_{MBP})_{fp}$ is the ratio among the number of lipids/MBP molecules in the fluorescent phase and A_{lip} is the average molecular area of the lipids.

We thank Dr. R. G. Oliveira for contributions to this work. We are deeply indebted to Drs. P. Rodriguez and K. Mitzutamari for help in obtaining some of the components used.

This work was supported in part by Secretaría de Ciencia y Técnica de la Universidad Nacional de Córdoba, Secretaría de Ciencia y Técnica, Fondo Nacional de Ciencia y Técnica, and Consejo Nacional de Investigación en Ciencia y Técnica (Argentina). C.M.R. is a Fellow and B.M. is a Career Investigator of the latter institution.

REFERENCES

1. Edidin, M. 2001. Shrinking patches and slippery rafts: scales of domains in the plasma membrane. *Trends Cell Biol.* 11:492–496.
2. Silvius, J. 2005. Lipid microdomains in model and biological membranes: how strong are the connections? *Q. Rev. Biophys.* 38:373–383.
3. Vereb, G., J. Szollosi, J. Matko, P. Nagy, T. Farkas, L. Vigh, L. Matyus, T. A. Waldmann, and S. Damjanovich. 2003. Dynamic, yet structured: the cell membrane three decades after the Singer-Nicolson model. *Proc. Natl. Acad. Sci. USA.* 100:8053–8058.
4. Fanani, M. L., S. Hartel, R. G. Oliveira, and B. Maggio. 2002. Bidirectional control of sphingomyelinase activity and surface topography in lipid monolayers. *Biophys. J.* 83:3416–3424.
5. Wang, J., A. Gambhir, G. Hangyas-Mihalyne, D. Murray, U. Golebiewska, and S. McLaughlin. 2002. Lateral sequestration of phosphatidylinositol 4,5-bisphosphate by the basic effector domain of myristoylated alanine-rich C kinase substrate is due to nonspecific electrostatic interactions. *J. Biol. Chem.* 277:34401–34412.
6. Honger, T., K. Jorgensen, R. L. Biltonen, and O. G. Mouritsen. 1996. Systematic relationship between phospholipase A2 activity and dynamic lipid bilayer microheterogeneity. *Biochemistry.* 35:9003–9006.
7. Cheng, K. H., B. Cannon, J. Metze, A. Lewis, J. Huang, M. W. Vaughn, Q. Zhu, P. Somerharju, and J. Virtanen. 2006. Lipid headgroup superlattice modulates the activity of surface-acting cholesterol oxidase in ternary phospholipid/cholesterol bilayers. *Biochemistry.* 45:10855–10864.
8. Muderhwa, J. M., and H. L. Brockman. 1992. Lateral lipid distribution is a major regulator of lipase activity. implications for lipid-mediated signal transduction. *J. Biol. Chem.* 267:24184–24192.
9. Hinderliter, A. K., A. R. Dibble, R. L. Biltonen, and J. J. Sando. 1997. Activation of protein kinase C by coexisting diacylglycerol-enriched and diacylglycerol-poor lipid domains. *Biochemistry.* 36:6141–6148.
10. Sackmann, E. 1995. Physical basis of self-organization and function of membranes: physics of vesicles. *In* Structure and Dynamics of Membranes: From Cells to Vesicles. R. Lipowsky and E. Sackmann, editors. Elsevier, North-Holland, The Netherlands. 213–298.
11. Hinderliter, A. K., J. Huang, and G. W. Feigenson. 1994. Detection of phase separation in fluid phosphatidylserine/phosphatidylcholine mixtures. *Biophys. J.* 67:1906–1911.
12. Shimshick, E. J., and H. M. McConnell. 1973. Lateral phase separations in binary mixtures of cholesterol and phospholipids. *Biochem. Biophys. Res. Commun.* 53:446–451.
13. Silvius, J. R. 1990. Calcium-induced lipid phase separations and interactions of phosphatidylcholine/anionic phospholipid vesicles. fluorescence studies using carbazole-labeled and brominated phospholipids. *Biochemistry.* 29:2930–2938.
14. Galla, H. J., and E. Sackmann. 1975. Chemically induced lipid phase separation in model membranes containing charged lipids: a spin label study. *Biochim. Biophys. Acta.* 401:509–529.
15. Denisov, G., S. Wanaski, P. Luan, M. Glaser, and S. McLaughlin. 1998. Binding of basic peptides to membranes produces lateral domains enriched in the acidic lipids phosphatidylserine and phosphatidylinositol 4,5-bisphosphate: an electrostatic model and experimental results. *Biophys. J.* 74:731–744.
16. Heimburg, T., and D. Marsh. 1995. Protein surface-distribution and protein-protein interactions in the binding of peripheral proteins to charged lipid membranes. *Biophys. J.* 68:536–546.
17. Epand, R. M. 2004. Do proteins facilitate the formation of cholesterol-rich domains? *Biochim. Biophys. Acta.* 1666:227–238.
18. Mouritsen, O. G., and M. Bloom. 1984. Mattress model of lipid-protein interactions in membranes. *Biophys. J.* 46:141–153.
19. Calderon, R. O., B. Maggio, T. J. Neuberger, and G. H. De Vries. 1993. Surface behavior of axolemma monolayers: physico-chemical characterization and use as supported planar membranes for cultured Schwann cells. *J. Neurosci. Res.* 34:206–218.
20. Oliveira, R. G., R. O. Calderon, and B. Maggio. 1998. Surface behavior of myelin monolayers. *Biochim. Biophys. Acta.* 1370:127–137.
21. Oliveira, R. G., and B. Maggio. 2000. Epifluorescence microscopy of surface domain microheterogeneity in myelin monolayers at the air-water interface. *Neurochem. Res.* 25:77–86.
22. Bernardino de la Serna, J., J. Perez-Gil, A. C. Simonsen, and L. A. Bagatolli. 2004. Cholesterol rules: direct observation of the coexistence of two fluid phases in native pulmonary surfactant membranes at physiological temperatures. *J. Biol. Chem.* 279:40715–40722.
23. Worthman, L. A., K. Nag, N. Rich, M. L. Ruano, C. Casals, J. Perez-Gil, and K. M. Keough. 2000. Pulmonary surfactant protein A interacts with gel-like regions in monolayers of pulmonary surfactant lipid extract. *Biophys. J.* 79:2657–2666.
24. Norton, W. T., and W. Cammer. 1984. Isolation and characterization of myelin. *In* Myelin. P. Morell, editor. Plenum Place, New York. 147–180.
25. Braun, P. E. 1984. Molecular organization of myelin. *In* Myelin. P. Morell, editor. Plenum Press, New York. 97–113.
26. Oliveira, R. G., M. Tanaka, and B. Maggio. 2005. Many length scales surface fractality in monomolecular films of lipids and proteins extracted form whole myelin. *J. Struct. Biol.* 149:158–169.
27. Oliveira, R. G., and B. Maggio. 2002. Composition domain immiscibility in whole myelin monolayers at the air-water interface and Langmuir-Blodgett films. *Biochim. Biophys. Acta.* 1561:238–250.
28. Rosetti, C. M., R. G. Oliveira, and B. Maggio. 2005. The Folch-Lees proteolipid induces phase coexistence and transverse reorganization of lateral domains in myelin monolayers. *Biochim. Biophys. Acta.* 1668:75–86.
29. Maggio, B., and F. A. Cumar. 1974. Antigen-dependent alterations in the lipid composition of the CNS in guinea pigs with experimental allergic encephalomyelitis. *Brain Res.* 77:297–307.
30. Monferran, C. G., B. Maggio, G. A. Roth, F. A. Cumar, and R. Caputto. 1979. Membrane instability induced by purified myelin components. Its possible relevance to experimental allergic encephalomyelitis. *Biochim. Biophys. Acta.* 553:417–423.
31. Rosetti, C. M., R. G. Oliveira, and B. Maggio. 2003. Reflectance and topography of glycosphingolipid monolayers at the air-water interface. *Langmuir.* 19:377–384.
32. Ali, S., H. L. Brockman, and R. E. Brown. 1991. Structural determinants of miscibility in surface films of galactosylceramide and phosphatidylcholine: effect of unsaturation in the galactosylceramide acyl chain. *Biochemistry.* 30:11198–11205.
33. Frey, W., W. R. Schief, Jr., and V. Vogel. 1995. Two-dimensional crystallization of streptavidin studied by quantitative Brewster angle microscopy. *Langmuir.* 12:1312–1320.

34. Miñones Jr, J., C. Carrera, P. Dynarowicz-Latka, J. Miñones, O. Conde, R. Seoane, and J. M. Rodriguez Patino. 2001. Orientational changes of amphotericin B in Langmuir monolayers observed by Brewster angle microscopy. *Langmuir*. 17:1477–1482.

35. Feng, S. 1999. Interpretation of mechanochemical properties of lipid bilayer vesicles from the equation of state or pressure-area measurement of the monolayer at the air-water or oil-water interface. *Langmuir*. 15:998–1010.

36. Phillips, M. C., D. E. Graham, and H. Hauser. 1975. Lateral compressibility and penetration into phospholipid monolayers and bilayer membranes. *Nature*. 254:154–156.

37. Sankaram, M. B., P. J. Brophy, and D. Marsh. 1989. Spin-label ESR studies on the interaction of bovine spinal cord myelin basic protein with dimyristoylphosphatidylglycerol dispersions. *Biochemistry*. 28:9685–9691.

38. Palmer, F. B., and R. M. Dawson. 1969. The isolation and properties of experimental allergic encephalitogenic protein. *Biochem. J*. 111:629–636.

39. Jo, E., and J. M. Boggs. 1995. Aggregation of acidic lipid vesicles by myelin basic protein: dependence on potassium concentration. *Biochemistry*. 34:13705–13716.

40. Boggs, J. M., and M. A. Moscarello. 1978. Structural organization of the human myelin membrane. *Biochim. Biophys. Acta*. 515:1–21.

41. London, Y., R. A. Demel, W. S. Geurts van Kessel, F. G. Vossenberg, and L. L. van Deenen. 1973. The protection of A1 myelin basic protein against the action of proteolytic enzymes after interaction of the protein with lipids at the air-water interface. *Biochim. Biophys. Acta*. 311:520–530.

42. Boggs, J. M., G. Rangaraj, and K. M. Koshy. 1999. Analysis of the membrane-interacting domains of myelin basic protein by hydrophobic photolabeling. *Biochim. Biophys. Acta*. 1417:254–266.

43. Bates, I. R., J. M. Boggs, J. B. Feix, and G. Harauz. 2003. Membrane-anchoring and charge effects in the interaction of myelin basic protein with lipid bilayers studied by site-directed spin labeling. *J. Biol. Chem*. 278:29041–29047.

44. Maggio, B., J. M. Sturtevant, and R. K. Yu. 1987. Effect of myelin basic protein on the thermotropic behavior of aqueous dispersions of neutral and anionic glycosphingolipids and their mixtures with dipalmitoylphosphatidylcholine. *J. Biol. Chem*. 262:2652–2659.

45. Fidelio, G. D., B. Maggio, and F. A. Cumar. 1984. Interaction of myelin basic protein, melittin and bovine serum albumin with gangliosides, sulphatide and neutral glycosphingolipids in mixed monolayers. *Chem. Phys. Lipids*. 35:231–245.

46. Harauz, G., N. Ishiyama, C. M. Hill, I. R. Bates, D. S. Libich, and C. Fares. 2004. Myelin basic protein-diverse conformational states of an intrinsically unstructured protein and its roles in myelin assembly and multiple sclerosis. *Micron*. 35:503–542.

47. Smith, R. 1992. The basic protein of CNS myelin: its structure and ligand binding. *J. Neurochem*. 59:1589–1608.

48. Ratto, T. V., and M. L. Longo. 2002. Obstructed diffusion in phase-separated supported lipid bilayers: a combined atomic force microscopy and fluorescence recovery after photobleaching approach. *Biophys. J*. 83:3380–3392.

49. Sankaram, M. B., P. J. Brophy, and D. Marsh. 1991. Lipid-protein and protein-protein interactions in double recombinants of myelin proteolipid apoprotein and myelin basic protein with dimyristoylphosphatidylglycerol. *Biochemistry*. 30:5866–5873.

50. Hollingshead, C. J., D. L. Caspar, V. Melchior, and D. A. Kirschner. 1981. Compaction and particle segregation in myelin membrane arrays. *J. Cell Biol*. 89:631–644.